Research Article

iMedPub Journals
http://www.imedpub.com

Endocrinology and Metabolism: Open Access

2021
Vol. 5 No. 5: 173

Real-Time Studies of Plasma Membrane Damage Trigger Cell Apoptosis from Sulfhydryl Nanoparticles

Ting Wang[1*], Guanwen Qu[2], Chenglong Cai[1,2], Yunyun Yue[3], Yaozhong Cheng[1], Boru You[1], Zhewei Shuai[1], Yixin Zhang[1], Zhangqi Feng[4], and Jing Shang[3]

[1]Department of Bioelectronics, State Key Laboratory of Bioelectronics, National Demonstration Centre for Experimental Biomedical Engineering Education, School of Biological Science and Medical Engineering, Southeast University, Nanjing, China
[2]Department of Bioelectronics, Jiangbei New Area Innovation Institute, Southeast University, Nanjing, China
[3]Department of Pharmacology, State Key Laboratory of Natural Medicines, China Pharmaceutical University, Nanjing, China
[4]Department of Chemical Engineering, School of Chemical Engineering, Nanjing University of Science and Technology, Nanjing, Jiangsu, China

Corresponding author: Ting Wang, Department of Bioelectronics, State Key Laboratory of Bioelectronics, National Demonstration Centre for Experimental Biomedical Engineering Education, School of Biological Science and Medical Engineering, Southeast University, Nanjing 210096, P. R. China

tingwang@seu.edu.cn

Citation: Wang T, Qu G, Cai C, Yue Y, Cheng Y, et al. (2021) Real-Time Studies of Plasma Membrane Damage Trigger Cell Apoptosis from Sulfhydryl Nanoparticles. Endocrinol Metab Vol. 5 No.5: 173.

Abstract

Background: Sulfhydryl groups are present on the surface of nanoparticles in unburned vehicle exhaust and most air pollutants produced by combustion, which raises the risk for exposure of human. Sulfhydride nanoparticles not only penetrate the skin range from the stratum corneum to pass below the dermis, they also entering the system is circulation from cell endocytosis pass way. The potential risk of skin and body healthy associated from sulfhydride nanoparticles were attach much attentions. It is important to illuminate the underlying toxicity of sulfhydride nanoparticles to human body, but the mechanisms underlying the toxicity of nanoparticles on cells remain unclear, especially the relationship from the damage of cells plasma membrane and the cell cycle.

Methods: We performed time-response studies and cells-membrane interaction studies in C6 cells to observe the effects of 50 nm and 200 nm sulfhydryl nanoparticles on the activities, cell metabolism and cell cycle. The cells were exposed to 0, 10 or 20 μg Nano particles for 12, 36, 24, 48 or 72 h to finish the particle response studies. On the time of treatment, cells were collected to assess the expression of tight junction-associated proteins, P21, FBW7 and cyclin E. To further investigate the mechanisms underlying nanoparticle-induced dysregulation of tight junction-associated protein, we studied the change of lipid bilayers. Sum frequency generation optic spectrum was carried out to study the membrane change.

Results: The results show that the smaller particles penetrate the plasma membrane and without bilayer disruption, whereas the larger one will pilled off one leaflet of the membrane, they are mostly trapped in endosomes. The larger ones result in slow but unrepairable cell necrosis and caused cell cycle regulation disorders *via* disturbing the expression of p21, cyclin E, and FBW-7.

Conclusion: The results suggest that the destruction of membrane structure by the particles will cause irreversible biological damage, and particles entering cells through protein assisted process will increase the expression of cell cycle related proteins and cells self-repair can be observed from the *in vitro* experiments. From the interactions between mitochondria lipid model and nanoparticles, we deduced that, the efficiencies of nano-scaled drugs could be enhanced by altering the interaction models of nano systems and mitochondria. In the future, mitochondria membrane proteins would also be carefully explored to confirm their roles in the active mitochondrial uptake of nanoparticles and provide new channels for safe and effective mitochondria targeting drug delivery. Real-time studies of plasma membrane damage from sulfhydryl nanoparticles, and analysis the triggering of cell apoptosis, will support safety assessment of nanoscale materials.

Keywords: Sulfhydryl nanoparticles; Plasma membrane; Lipid flip-flop; Self-repair; Cell cycle deregulation

Abbreviations: SFG: Sum Frequency Generation Spectrum; ROS: Reactive Oxide Species; d-DSPC: 1,2-distearoyl(d70)-sn-glycerol-3-phosphocholine-1, 1,2,2-d4-N,N,N-trimethyl-d9; DSPC: 1,2-distearoyl-sn-glycero-3-phosphocholine; POPC: 1-palmitoyl-2-oleoyl-glycero-3-phosphocholine.

Received: July 30, 2021; **Accepted:** August 13, 2021; **Published:** August 20, 2021

Introduction

Nano-objective has many opportunities to contact or be used with organisms. Many drug delivery systems were designed to target to the cytosol or nucleus of cells during the process passage through the cells membranes to reach the target compartment. In this process, efficient delivery and avoiding cytotoxicity must be achieved. In this manner, understanding the mechanisms of nanoparticle-membrane interaction would be the key to designing potent cell-membrane-penetrating drugs.

Most groups studied cytotoxicity of nanoparticles with different modifications. It is often result from organelle targeting and damage. The organelle dynamics influenced by intrinsic properties of nanoparticles, such as their size, shape, and surface functional groups. But the cell and organelle membrane respond of drug delivery, especially the membrane permeability of nanoparticles, played essential roles when nanoparticles interacted with cells. Drug delivery such as nano particles could enter cell organ through different channels: protein import channels, permeability transition pores, mitochondrial apoptosis related channels (MACs), apoptosis-related ceramide pores, and the processes will possible preparative damage to the cell organ membrane. For example, mitochondria-targeting drug delivery was considered related with depolarization of mitochondrial and this process induced therapeutic agents and antioxidants effected with cells and animals [1,2]. However, cell organ depolarization closely related with membrane structure change. Growing numbers of groups studied dynamics process between cells and nanoparticles such as change of lipid bilayer or mitochondria membranes damage. But the mechanisms of lipid membrane change from nanoparticles are still hard to be described.

In our former works, the reversible and irreversible mitochondria damages caused by cationic and neutral silica nanoparticles were well discussed respectively and those mitochondrial injuries finally resulted in the unbalance of the cell cycle regulation network and severe cell cycle arrests [3-5]. Considering negatively charged nanoparticles were favourably used as drug deliverer based on mitochondria targeting, further steps for negatively charged nanoparticles were then focused on the presented research [4,5].

In this work, SiO_2 nanoparticles with different size (50 nm and 200 nm) were functionalized with sulfhydride groups for negative surface charges. The two sizes of nanoparticles presented different cell-nanoparticle interactions models, especially different processes when interacting with the mitochondrial membrane. Furthermore, cell fate changes, including cell cycle changes and cell cycle regulation network fluctuations were also detected. P21, cyclin E, and FBW-7 abundances were specially measured as identifiers of G1 and S phase progresses. This work will address the mechanisms of nanoparticle toxicity, based on NPs and mitochondrial membrane interactions, to support safety assessment of nanoscale materials.

Materials and Methods

Characterization of sulfhydride nanoparticles

Size, shape, and surface charges of 50 nm and 200 nm sulfhydride silica nanoparticles were firstly confirmed for further experiments. Size distributions and ζ-potentials in PBS of 50 nm and 200 nm sulfhydride silica nanoparticles were analyzed using Zetasizer Nano ZS (Malvern Panalytical). Infrared Spectroscopy (NICOLET iS50 FT-IR) was used to distinguish the sulfhydride groups on the SiO2 particle samples. For IR examination, aminated and alkylated nanoparticles were dehydrated under an infrared lamp, and then the dried particles were embedded with potassium bromide (KBr) and tableted to ~100 nm thick films for further Infrared Spectroscopy. Infrared Spectra was acquired at 2 cm^{-1} resolution.

Sum Frequency Generation (SFG) assay

We then studied model cell membrane and SiO2/NPs interactions by SFG and supported lipid bilayers. Details regarding SFG experiment set-up and SFG theory are published and will not be repeated here [6-9]. Using SFG and isotopically asymmetric lipid bilayers we can observe molecular interactions between the particles and each leaflet by monitoring the C-H and C-D stretching signals. Asymmetric double layer of 1,2-distearoyl(d70)-sn-glycerol-3-phosphocholine-1, 1,2,2-d4-N,N,N-trimethyl-d9 (d-DSPC) and 1,2-distearoyl-sn-glycero-3-phosphocholine (DSPC) lipid bilayers (d-DSPC-DSPC) were prepared as model cell membranes, the chemical structures of d-DSPC and DSPC were show in **Figure S1**. To study the interactions between SiO2 and each leaflet of the lipid bilayer, SFG spectra were collected from the lipid bilayers with d-DSPC as outer leaflet and DSPC as inner leaflet. SFG spectra collected from the lipid bilayers before and after the addition of nanoparticles to the sub-phase of the bilayers.

To avoid the overlap of signals in the C-H stretching frequency region we developed symmetric double layer of 1-palmitoyl-2-oleoyl-glycero-3-phosphocholine (POPC) lipid bilayer, chemical structures were show in **Figure S2**. SFG only detects signals from media without inversion symmetry. SFG intensity can hardly be observed from POPC-POPC due to their approximate inversion symmetry. After SiO_2 particles were added into the sub-phase in contact with the lipid bilayers, the lipid bilayers will be interacted with the particles. Therefore strong SFG signals were detected in the C-H stretching frequency range (between 2800 and 3000 cm^{-1}).

In vitro analysis

Rat glioma cell line C6 was used to test the cell responses to sulfhydride nanoparticles. Cells were cultured in High Glucose Dulbecco's Modified Eagle Medium (High Glucose DMEM, KeyGEN BioTech, China) with 10% Fetal Bovine Serum (FBS) under 37°C, 5% CO_2 .

For confocal microscope observation, cells were seeded in 96-well confocal plates and treated with 50 nm and 200 nm sulfhydride nanoparticle at a concentration of 5 μg/1,000 cells for 8 hrs, 16 hrs, 24 hrs, and 32 hrs. After being co-cultured with nanoparticles, cells were washed three times with Phosphate Buffered Saline (PBS) and stained with 50 nM MitoTrackerTM Green FM (488 nm, ThermalFisher Scientific, US) and LysotrackerTM Deep Red (638 nm, ThermalFisher Scientific, US) under 37°C, 5% CO_2 for 20 min to label mitochondria and lysosome, respectively. Then cells were washed with PBS three times and then cultured in serum-

free DMEM and observed under TCS SP8 confocal laser scanning microscope (Leica, Germany). Nanoparticles were visualized with RT (15/85) gate [10].

For flow cytometry assays, nanoparticles were seeded in 6-well culture plates and treated with 50 nm and 200 nm sulfhydride nanoparticle at a concentration of 5 μg/1,000 cells for 8 hrs, 16 hrs, and 24 hrs. Scattering light intensity was used to define the endocytosis of nanoparticles. Three independent repetitions were collected in each group, and 50,000 cells were counted in each sample. Reactive oxide species (ROS) production caused by 50 nm and 200 nm sulfhydride nanoparticles were detected using ROS Assay Kit (Beyotime Biotechnology, China). Three independent repetitions were collected in each group, and 50,000 cells were counted in each sample. Cell apoptosis under the effects of 50 nm and 200 nm sulfhydride nanoparticles were detected using Cell Apoptosis Kit (KeyGEN BioTech, China). Three independent repetitions were collected in each group, and 100,000 cells were counted in each sample. Cell cycle changes caused by 50 nm and 200 nm sulfhydride nanoparticles were examined using the Cell Cycle Assay Kit (Beyotime Biotechnology, China). Three independent repetitions were collected in each group, and 100,000 cells were counted in each sample. All flow cytometry assays were run on NovoCyte 2060R (ACEA Bioscience Inc. USA), fluorescence calculation, and fitting were conducted on NovoExpress (ACEA Bioscience Inc. USA).

Western blot assay

For western blot assay, 1,000,000 cells were seeded in 6-well plates and treated with 50 nm and 200 nm sulfhydride nanoparticles for 24 hrs and 48 hrs. After the nanoparticles were washed out, cells were gathered, washed, and suspended in cold PBS and then lysed in Cytobuster TM Protein Extraction Reagent (Novagen, USA) at 4°C for 30 min. After centrifugation at 12,000 rpm under 4°C for 20 min, the protein was extracted in the supernate. Extracted protein concentrations were then quantified *via* the BCA method. And then protein (≤ 40 μg) were resolved by 10% SDS-polyacrylamide gel electrophoresis and transferred electrophoretically to polyvinylidene difluoride (PVDF) membranes and then were blocked overnight in 5% skim milk in TBST (containing 20 mM Tris-HCl pH 7.4, 100 mM NaCl, and 0.1% Tween 20) buffer at 4°C. After washed in TBST buffer, they were then incubated with anti-Cyclin E1-cdk 2 polyclonal antibody ((ab71535), Abcam, USA), anti-FBW7 antibody ((ab192328), Abcam, USA), anti-p21 antibody ((ab109199), Abcam, USA)), respectively as the primary antibodies overnight, and then incubated with the HRP* Goat anti-Rabbit IgG secondary antibody (ImmunoWay, USA) for 3 h. After incubation, the bands were then detected using the ECL Prime Western Blotting Detection System (BioRaD, USA), and the grey-scale was analyzed by Gel-pro analyzer 4.0.

In vivo experiments

AB wild-type strain was used in this study. All lines were purchased from China Zebrafish Resource Center (CZRC, China). All studies involving animal manipulations were approved by the Institutional Animal Use and Care Committee of Nanjing Ruiying Runze Biopharmaceutical Technology Co., Inc. and followed the National Institutes of Health guidelines for the care and use of animals. 50 nm and 200 nm sulfhydride silica nanoparticles were co-cultured with zebrafish eggs at a concentration of 10 μg/mL respectively. The fishes were hatched out after 48 hrs co-incubation with the two kinds of nanoparticles and continually these newly hatched zebrafishes were co-incubated with 10 μg/mL 50 nm and 200 nm nanoparticles respectively for seven days. The survival and mutation of eggs and fished were observed under the microscope.

Results

Nanoparticles properties

Cell internalization process of nanoparticle: In this part we analysis cellular internalization of nanoparticles and the relationship with their properties. The shape, size, and surface charges of 50 nm and 200 nm sulfhydride nanoparticles were detected to determine the cell internalization process of nanoparticles. IR spectrum shown the sulfhydride groups on nanoparticles **(Figure 1a)**, dynamic laser light scattering shown the size distribution of the nanoparticles were 50 ± 5 nm and 200 ± 20 nm **(Figure S1)**. ζ-potentials of the nanoparticles were -38.033 ± 5 mV and -24.900 ± 5 mV, the surface charge densities were -4.845×10^{-3} mV/nm^2 and -1.982×10^{-4} mV/nm^2.

With the scattering light from nanoparticles, we quantified the intercellular nanoparticles **(Figure 1b)**, the maximum number of nanoparticles can be found at 8 h, but the amount of nano particles decreased when the time increased from 8 hrs to 32 hrs, mappings of scattering light results can be found in **Figure S1**. As it was shown in the literature [3-5], with the cell's differentiation, the number of internalized nanoparticles gradually decreased. It was based on the cells proliferation and the relative quantity decrease of the particles. And in this experiment, the internalized particles with the size of 50 nm was found have larger quantities than the 200 nm sized nanoparticles at 8 hrs but they metabolized faster than 200 nm sized nanoparticles in 32 hrs.

Then cell internalization processes of nanoparticles were assessment, from **Figure 1c**, we found that both of the nanoparticles with different size will enter cells membrane and they can be found in the cells cytoplastic. From the confocal images as show in **Figure 1c**, nanoparticles with the size of 50 nm will accumulation around the cell's nucleus, far from the cells membrane. In the confocal image, particles with diameter of 50 nm cannot be found from the top scan but they can be observed from the side scan. The nanoparticles with the size of 200 nm can be found close to the cells membrane, and some of the particles are on the top of cells membrane that can be clear observed from top scan of confocal. We suggest that the different distribution and metabolism of the nanoparticles in cells was from the different endocytosis and exocytosis processes of nanoparticles. The interactions between the particles and cell membranes will be important to understanding the process. So, Sum Frequency Generation Spectrum (SFG) was used as a monolayer lipid analysis method for the interactions of nanoparticles/cells membrane studies.

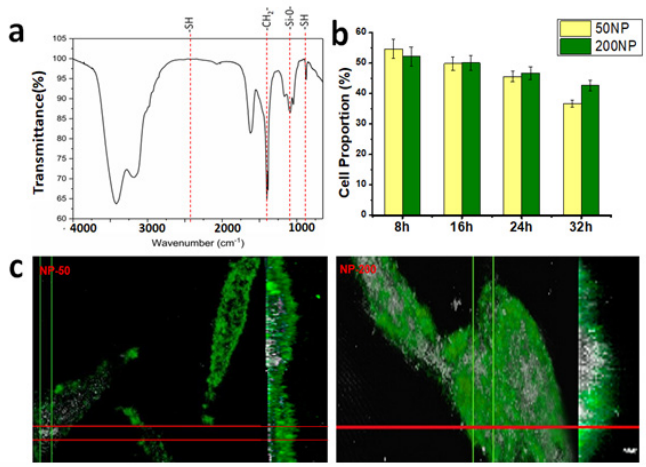

Figure 1: (a) IR results of 50 nm and 200 nm sulfhydride silica nanoparticles; (b) The SSC intensity for cells proportion at different time point; (c) Confocal images for intercellular of nanoparticle, NP-50 was the nanoparticles with size of 50 nm, NP-200 was the nanoparticles with size of 200 nm.

SFG assay of the interactions between nanoparticles and model lipid membrane

Nanoparticle entering organelle such as mitochondria against bio-membrane potential were considered dependent on the membrane flip-flop process (protein-free) or transport proteins (protein-assisted) on mitochondria. To detect the transmembrane movements of nanoparticles between the two leaflets of a cell membrane from the protein-free or protein-assisted manners, sum-frequency generation vibrational spectroscopy was used to observe the direct interactions between nanoparticles and lipid membrane **(Figure S2)**.

Previous studies had shown that Sum-Frequency Generation (SFG) vibrational spectroscopy provided a direct method to examine phospholipid flip-flop without labelling [11-14]. The wavelength ranges from 2000~2300 **(Figure 2a)** was from d-DSPC **(Figure S2)**, it was obtained to avoid the noisy from the inner leaflet of DSPC **(Figure S2)** and to avoid the noisy from the particles. From the results it can be observed that when the particles interacted with the lipid bilayer, the signals of d-DSPC dropped off with the quantities of particles increasing from 20 μg to 60 μg.

To know whether 200 nm nanoparticles had the similar influences on the phospholipid membrane of the liquid phase, the influences of 200 nm nanoparticles on POPC/POPC phospholipid membrane were studied **(Figure 2b)**. The symmetrical two leaflets of POPC/POPC phospholipid could not show SFG intensity with their symmetry structures **(Figure 2b** blue line **)**. However, when the lipid membrane interacted with the nanoparticle, one leaflet of the bilayer were damaged by the nanoparticles the other leaflet of lipid bilayer keep in order, and asymmetry structures of phospholipid were formed, SFG signal enhancement could be found **(Figure 2b red line)**. The results suggested that tilts, turn or other actions happened on one of the leaflets when the lipid bilayer interacted with the nanoparticles.

To further understanding the interaction process between nanoparticles and the lipid bilayers, we quantified the speed of the lipid bilayer flip-flop under the influence from nanoparticles.

In the absence of external interference, the lipid bilayer flipped spontaneously at a stable rate, which could be determined directly from the SFG intensity of CH_3 asymmetric stretching vibration on lipid bilayers. To understanding the spontaneously flipping of the membrane will be very important for us to understanding the process of membrane flip-flop under affection from nanoparticles. The time-dependent CH_3 asymmetric stretching vibration intensity could be simplified to the following function [15]:

$$I_{CH3}(t)=I_{R,max}e^{-4kt}+I_{R,min} \quad (1)$$

Where "IR, max" and "IR, min" were the maximum and minimum resonant CH_3 asymmetric stretching intensity, and k was the intrinsic rate of lipid flip-flop, which was determined by fitting function (1) to the CH_3 asymmetric stretching vibration intensity. Conversely, if the decay curve of CH_3 asymmetric stretching vibration intensity could be fit by an exponential function, the lipid must be flipped at a stable rate.

The kinetics of DSPC flip-flop was determined by continuously monitoring the CH_3 asymmetric stretching vibration intensity from the lipid DSPC as a function of time in the presence of nanoparticles. **Figure 2c** showed a representative decay curve for 60 μg of 200 nm nanoparticles added to the d-DSPC/DSPC bilayer at 0 sec to 2000 sec. To obtain the kinetic rate of DSPC flip-flop, the decay curve was fit by a single exponential function:

$$y=9.74708\ e^{-0.00314x}+0.82359 \quad (2)$$

As it was reported, in room temperature the d-DSPC/DSPC phospholipid would be very stable and intrinsic rate k would be hard to be observed. When the temperature increased to 41°C, d-DSPC/DSPC phospholipid will turn flip-flop and the intrinsic rate k was 1.85 × 10-5 [16]. In our experiment, NPs of 200 nm were used to influence the d-DSPC/DSPC phospholipid, time-dependent CH_3 intensity of d-DSPC was analysis **(Figure 2c)**. We calculated from equation 1, the intrinsic rate k was 7.85 × 10^{-4} s^{-1} . Comparing with that, the spontaneous flip-flop rate of d-DSPC/DSPC phospholipid in 41°C was an order-of-magnitude slower. So, it could be considered that in room temperature, the phospholipid membrane flip-flop was only influenced by the particles, while the spontaneous flip-flop rate was negligible. From the result, we found that 200 nm nanoparticles tended to flip the d-DSPC/DSPC phospholipid membrane at a stable rate and significantly alter the rate of Trans bilayer movement. Details of d-DSPC/DSPC phospholipid signals were described by the SFG curve **(Figure 2c and 2d)**.

The time-dependent CH3 intensity of POPC-POPC phospholipid membrane was shown in **Figure 2d**. It was clear that 200 nm nanoparticles had great influences on the rate of POPC-POPC phospholipid membrane flip-flop. To verify the intrinsic rate of membrane flip-flop, we made a simple coordinate transformation, as shown in **Figure 2d***. The curve was fit by exponential function:

$$y=3.11736e^{-0.00227x}+2.59678 \quad (3)$$

The result showed that the POPC/POPC membrane influenced by 200 nm nanoparticles was flipped at a stable rate, and the rate k was $5.68 \times 10^{-4} s^{-1}$, which was also much larger than that of phospholipid membrane spontaneous flip-flop.

Deduced from SFG result, 200 nm nanoparticles changed the monolayer of the phospholipid by flipping or peeling one of the leaflets and led to intensity signals increasing or dropping. In summary, 200 nm nanoparticles could significantly alter the rate of phospholipid membranes movement. And for phospholipid membrane of solid or liquid phases, turn, tilt, and other disturbs both can be found on one of the leaflets.

50 nm nanoparticles were also studied, the results showed that 50 nm nanoparticles did not flip the DSPC-dDSPC phospholipid membrane at a stable rate and the fluctuation of CH_3 intensity was relatively small **(Figure 2e)**. This result indicated that 50 nm nanoparticles had little influence on the flip-flop of the phospholipid membrane; they could not flip or peel the monolayer of phospholipid membrane as the nanoparticles of 200 nm.

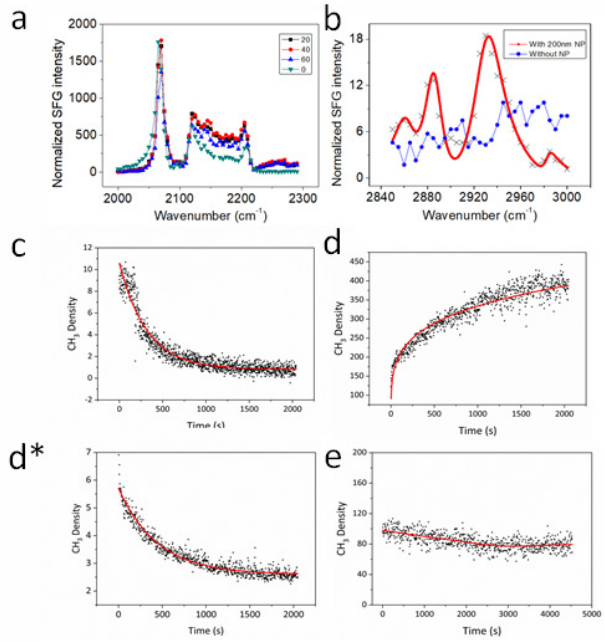

Figure 2: (a) Details of d-DSPC/DSPC phospholipid signals when interacted with different concentration (20 μg to 60 μg) of 200 nm silica particles; (b) Details of POPC/POPC membrane with 200 nm silica particles (60 μg); (c) Representative decay for d-DSPC/DSPC bilayers with 60 μg of 200 nm silica particles adding at the 0 s; (d) Metadata of CH3 intensity of POPC/POPC membrane with 20 μg of 200 nm silica particles added at the 0 s as a function of time; (d*) Coordinate transformation of metadata of POPC/POPC with silica particles in sketch of 200 nm nanoparticle interacting with the lipid membrane; (e) 60 μg of 50 nm silica particles were added to the d-DSPC/DSPC phospholipid membrane at the 0 s.

In conclusion, SFG results proved that 50 nm nanoparticles cannot influence the lipid membrane, while, when the phospholipid membrane interacted with 200 nm nanoparticles, disturbance on one leaflet of the phospholipid membrane could be found. But the 200 nm nanoparticles could not disturb both leaflets of the lipid membrane from flip-flop processes. 200 nm nanoparticles would scrape the mitochondria membrane violently. It can be deduced from the results that the transmembrane delivery process will be different for different size nanoparticles. It will lead to different cell dynamics and stress responses. It would be very interesting to further study the cellular network and cellular metabolisms when they underwent the treatments of different types of nanoparticles. In next step we tried to determine the cell toxicology mechanism of different nanoparticles by combining SFG optical analysis and biochemistry studies.

Subcellular localization of 5 nm and 2 nm nanoparticles

50 nm and 200 nm sulfhydride silica nanoparticles were co-cultured with C6 cells for 8 hrs, 16 hrs, 24 hrs, and 32 hrs. Side Scattered Light (SSC) from flow cytometry assay revealed that the cellular uptake of both kinds of nanoparticles increased with time extending within 24 hrs. It can be deduced from the results **(Figures S1, S3 and S4)** that more 50 nm nanoparticles were internalized than 200 nm ones within the same period. However, SSC results also show that small quantities of 200 nm particles lead to much serous organelle damages and organelle fragmentation rarely can be found with large quantities of 50 nm nanoparticles. Further studies from confocal microscope were carried out to explore the subcellular distributions of different nanoparticles we tried to determine the cell toxicology mechanism of different nanoparticles from biochemistry studies.

As is shown in **Figure 3**, 50 nm nanoparticles were mainly observed in the cytoplasm within 32 hrs. Though lysosome was not found co-localize with 50 nm nanoparticles, they were injured or swollen (white dash circles in **Figure 3**) after 24 hrs and 32 hrs co-incubation with these nanoparticles. Moreover, 50 nm nanoparticles were found to keep adhering to mitochondria, and a few of them also entered mitochondria after 24 hrs and 32 hrs co-incubation (yellow arrows in **Figure 3**) and this phenomenon was considered caused mitochondria deformation as well (yellow dash circles in **Figure 3**).

From **Figure 3**, 200 nm nanoparticles were also mainly found in the cytoplasm within 32 hrs. However, different from 50 nm ones, 200 nm nanoparticles entered lysosomes after 16 hrs co-incubation (white arrows in **Figure 3**) and induced increasingly serious lysosome injuries during 16 hrs-32 hrs (white dash circles in **Figure 3**). Interestingly, 200 nm nanoparticles was found kept close attachments to mitochondria but cannot be found internalization by mitochondria. From the results of SFG optical analysis, it was proved that, large sized nanoparticles (200 nm) can damage one leaflet of lipid bilayer in a speed way. We suggested that will be the main reason the large particles can entry the lysosomes composed with monolayers at a short time. At the same time, SFG results proved that they cannot damage both leaflet of the lipid bilayers, so they hardly can be internalization by mitochondria, since the barrier of monolayer on mitochondria membrane blocked the particles entering. However, the damage of monolayer at mitochondria resulted in their deformation that can be found at 24 hrs and 32 hrs.

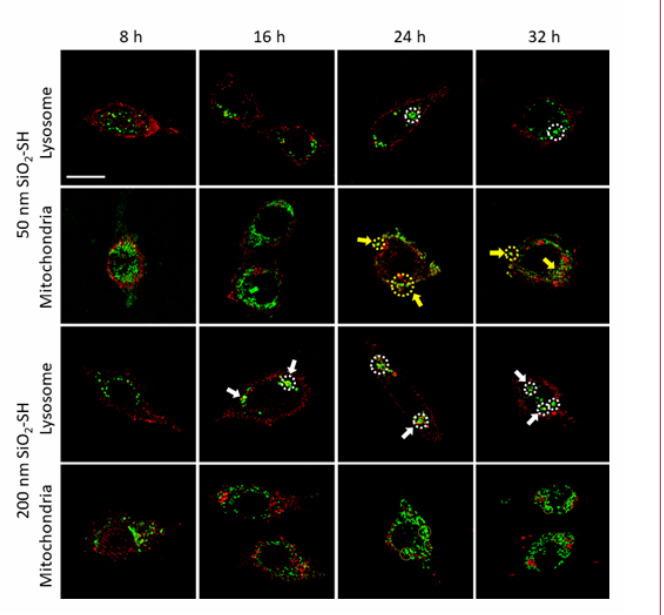

Figure 3: The confocal images of C6 cells after being co-incubated with 50 nm (first and second row) and 200 nm (third and fourth row) sulfhydride nanoparticles for 8 hrs, 16 hrs, 24 hrs, and 32 hrs. Nanoparticles were labelled with red, and lysosomes were labelled with green (first and third row), and mitochondria were labelled with green (second and fourth row). White dashed circles presented the lysosome deformations, and white arrows pointed to the co-localizations of nanoparticles and lysosomes. Yellow dashed circles presented the mitochondria deformations, and yellow arrows pointed to the co-localizations of nanoparticles and mitochondria. Scale bar=10 μm.

Comprehensively, 50 nm and 200 nm nanoparticles presented different subcellular localizations, since they underwent different subcellular transport pathways. It was well known that, lysosome is a low-pH organelle, which was always used as a target organelle for pH-triggered nanoparticles. In our experiments, it was found that 50 nm nanoparticles tended to escape from the lysosome uptake process due to their smaller sizes. The particles with 200 nm would reach lysosomes at the end of the endocytosis process; however, this process cannot result from the pH-triggered property, but the kinetic process that was proved damaged monolayer of phospholipid membrane.

The interactions between nanoparticles and mitochondria were more complex. 50 nm and 200 nm nanoparticles can be found aggregated around mitochondria, it was considered that the protons pump process, H+ transport and proton gradient of mitochondria appear critical to the particle aggregation. After 24 hrs, nanoparticles of 50 nm were found entered mitochondria against membrane potential. The SFG results show that small particles of 50 nm cannot flip the DSPC-dDSPC phospholipid membrane. Without flipping or peeling any leaflet of the phospholipid bilayer, the only way that the 50 nm particles could be internalized into mitochondria was considered to be *via* proteins assistant process. As for 200 nm nanoparticles, from light scattering and co-location images it can be found that 200 nm nanoparticles can hardly penetrated the mitochondria. From SFG results, 200 nm nanoparticles just can peel off one leaflet of the membrane that is why we cannot find 200 nm nanoparticles penetrated the mitochondria. With the influences from 200 nm nanoparticles, the mitochondria fusion could be observed in **Figure 3**, which must result from one leaflet of the phospholipid membrane peeled or flipped by 200 nm nanoparticles.

Influence of different sized sulfhydride nanoparticles and their toxicity for cells should be deeply illuminated. We analysis the ROS, cell apoptosis and cell cycle in further studies.

ROS production

Reactive Oxide Species (ROS) production in cells was detected to estimate the oxidative stress caused by 50 nm and 200 nm sulfhydride nanoparticles. Flow cytometry was carried out to illustrate ROS productions under the influence of two kinds of nanoparticle treatment. And fluorescence intensities within 102-103 were counted as strong ROS release. To eliminate false-positive caused by washing and centrifuging, the average fluorescence intensity of within 102-103 of the control group was deducted in experiment groups.

According to **Figure 4a**, both 50 nm and 200 nm nanoparticles induced instant ROS production within 1 hr, and 200 nm nanoparticles induced more ROS release than the 50 nm ones. After 24 hrs, ROS productions caused by 50 nm nanoparticles did not change significantly, while ROS production caused by 200 nm decreased to similar to 50 nm nanoparticle group. According to the results, cells reacted rapidly to both 50 nm and 200 nm nanoparticles, and 200 nm nanoparticles could induce more violent ROS release. Moreover, the ROS response induced by the two kinds of nanoparticles would converge and maintain for at least 24 hrs.

As is widely accepted, mitochondria damages are highly correlated with oxidative stress. 200 nm nanoparticles were observed to peel one of the leaflets in the mitochondrial lipid bilayer, as well as to induce acute and violent ROS production. So, it was suggested that flip-flop on one leaflet lipid of the mitochondrial membrane caused mitochondria damages and mitochondria-derived ROS aggravated. For the 50 nm nanoparticles, injuries of mitochondria from particle-invasions could be found without lipid membrane disturbance. But the ROS productions from 50 nm nanoparticles were significantly slighter than those caused by 200 nm nanoparticles **(Figure 4)**, even though varying degrees of mitochondria damages can be found in both of the groups (yellow dashed circles in **Figure 3**). These results deduced that protein-dependent mitochondrial penetration reduced acute ROS release and mitochondria injuries at the same time the damage of mitochondria membrane will increase ROS release. In conclusion, 200 nm nanoparticles induced more mitochondria-derived ROS, due to peeling one leaflet of the mitochondria membrane and causing serious mitochondrial damage. Mitochondria injuries and mitochondria-derived ROS would attack bio-macromolecules such as DNA and protein as well as organelle dysfunction, which manifested cell metabolism changes and even necrosis and apoptosis [17].

Cell apoptosis assay

Cell apoptosis assay after 24 hrs and 48 hrs caused by 50 nm and 200 nm sulfhydride silica nanoparticles was conducted *via* flow cytometry **(Figure 4b)**. According to the results, 50 nm caused late apoptosis and severe cell necrosis. From 24 hrs to 48 hrs, both late apoptosis and necrosis decreased obviously. For 200 nm nanoparticles, during 24 hrs, both of the late apoptosis and cell necrosis were not severe as those caused by 50 nm nanoparticles. After 48 hrs, the late apoptosis caused by 200 nm nanoparticles almost did not change, while necrosis increased rapidly.

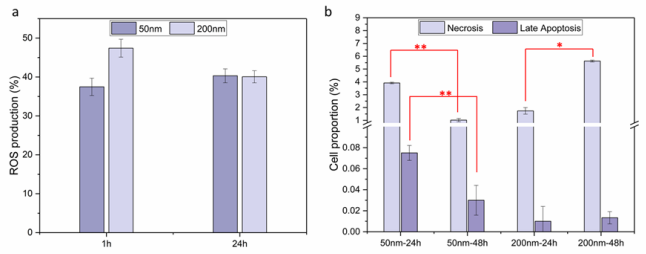

Figure 4: (a) ROS release and (b) cell apoptosis assay results of cell treated with 50 nm and 200 nm nanoparticles.

The execution and propagation of cell necrosis were well described to be correlated with ROS, which also provoked damages to proteins, lipids, and DNA [18]. Interestingly, 50 nm nanoparticles caused lower ROS production from 1 hr to 24 hrs; however, they induced higher cell necrosis in 24 hrs. The results indicated that, 50 nm nanoparticles actively internalized by mitochondria and lead to mitochondria dysfunction following mitochondria deformation (yellow dashed circles in **Figure 3**) triggering apoptosis. From 24 hrs to 48 hrs, decreasing cell death was observed caused by 50 nm nanoparticles, suggested that necrosis induced by 50 nm nanoparticles could be gradually alleviated. We deduced from the results that the biomolecule damages along with cell recovering were also partially repaired. Differently, 200 nm nanoparticles induced more severe ROS production but less severe necrosis than 50 nm nanoparticles did. We suggest that one leaflet of the lipid flip-flop on the mitochondrial membrane caused mitochondria damages and mitochondria-derived ROS aggravated. At the same time, lysosome deformation (white dashed circles in **Figure 3**) also contributes to the quick ROS release. At 48 hrs, a large number of necrosis cells can be found deduced that mitochondria-derived ROS aggravated caused by 200 nm nanoparticles could result in slower but unrepairable mitochondria damages, so that the affected cells underwent slow but deteriorating necrotic pathways.

Cell cycle assay

Most cells adjusted themselves to survive under the pressure of 50 nm and 200 nm sulfhydride nanoparticles. Cell cycle changes after 24 hrs and 48 hrs caused by 50 nm and 200 nm sulfhydride silica nanoparticles were assessed by flow cytometry, and results were shown in **Figure 5**. Treated with 50 nm nanoparticles for 24 hrs, cells presented obvious G1 phase prolongation, but S phase did not change sharply. After 48 hrs treatment, G1 phase restored, while S phase extended significantly. Treated with 200 nm nanoparticles for 24 hrs, cells presented obvious G1 phase prolongation and slight S phase shorten. After 48 hrs treatment, G1 phase arrest alleviated slightly but S phase prolonged remarkably. Comprehensively, 50 nm nanoparticles caused significant G1 phase arrest within 24 hrs. In this stage, limited cells were able to pass the G1/S checkpoint, because large quantities of cells were arrested in the G1 phase due to undesired intracellular environment, including organelle injuries, ROS release and DNA damages. From 24 hrs to 48 hrs, the G1 phase recovered obviously while S phase prolonged, which means in this stage, with some self-recovery mechanism, cells arrested in the G1 phase overpassed the G1/S checkpoint and entered the S phase. Nevertheless, some severe genome and protein damages caused by ROS release in mitochondria and lysosome injuries were not fully healed, so these cells still could not finish the DNA replication and were arrested in S phase. From the results, we suggested that the 50 nm nanoparticles, which were actively internalized by mitochondria, caused partially repairable metabolism disorders, and cells would initiate an obvious self-repair process.

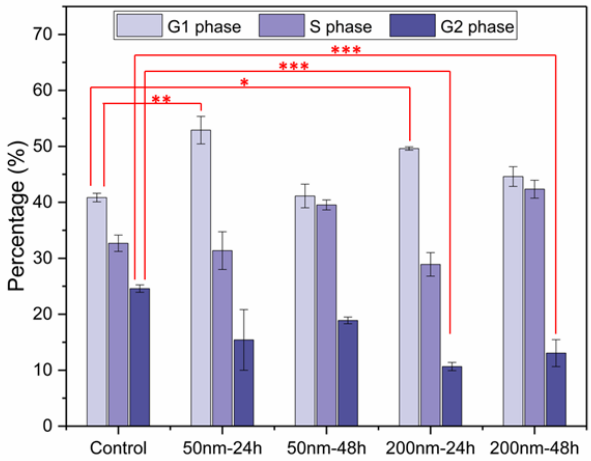

Figure 5: Cell cycle assay results of cells treated with 50 nm and 200 nm nanoparticles for 24 hrs and 48 hrs.

Regarding 200 nm nanoparticles, they also caused G1 phase arrest within 24 hrs, which indicated that organelle injuries, ROS release and DNA damages were also caused by the 200 nm nanoparticles. From 24 hrs to 48 hrs, G1 phase arrest recovered slightly, which suggested that though some of the cells arrested in the G1 phase passed the G1/S checkpoint, most of these cells were still arrested in the G1 phase. Simultaneously, the cells entered the S phase also could not complete DNA replication and be detained in the S phase. These disordered G1/S transition and S phase progress were attributed to the DNA and protein damages, which followed mitochondrial membrane disturbance **(Figures 1 and 2)** caused by 200 nm nanoparticles.

Western blot assay

The changes in the cell cycle regulation system could be the underlying reasons for the cell cycle changes of C6 cells under the effects of 50 nm and 200 nm sulfhydride silica nanoparticles.

Therefore, the abundances of p21, cyclin E, and FBW-7, which were key mediators in the G1 phase and S phase, were measured and presented in **Figure 6.**

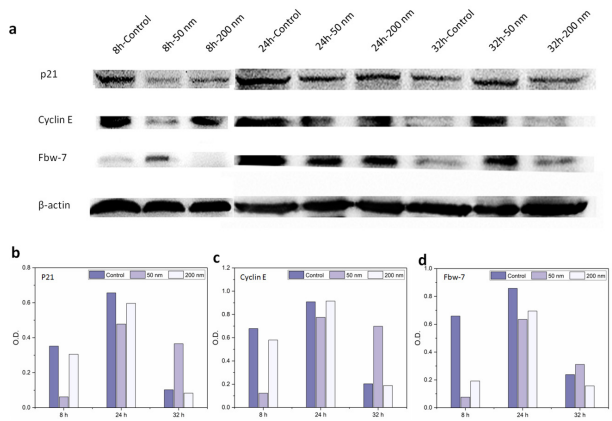

Figure 6: (a) WB results show the quantities of P21, cyclin E and Fbw-7; (b) P21 abundance; (c) cyclin E abundance and (d) FBW-7 abundance of healthy cells and cells treated with 50 nm and 200 nm nanoparticles.

Regarding p21, its abundance in normal C6 cells increased from 8 hrs to 24 hrs and then dropped steeply from 24 hrs to 32 hrs. After co-incubated with 50 nm nanoparticles, p21 abundance was significantly lower than the control group in 8 hrs. And then p21 abundance increased from 8 hrs to 24 hrs but decreased slightly from 24 hrs to 32 hrs. Differently, after co-incubated with 200 nm nanoparticles for 8 hrs, p21 abundance was only slightly lower than the control group. And then p21 abundance increased from 8 hrs to 24 hrs but decreased significantly from 24 hrs to 32 hrs.

As for cyclin E, in the control group, cyclin E doubled from 8 hrs to 24 hrs and then decreased steeply from 24 hrs to 32 hrs. After being co-incubated with 50 nm nanoparticles, cyclin E abundance was incredibly lower than the control group in 8 hrs. And then cyclin E abundance increased to almost 10-folds from 8 hrs to 24 hrs, and then decreased slightly from 24 hrs to 32 hrs. Besides, affected by 200 nm nanoparticles, cyclin E abundance was lower than the control group in 8 hrs. And then cyclin E abundance increased incredibly from 8 hrs to 24 hrs, and decreased steeply from 24 hrs to 32 hrs.

Regarding FBW-7 in the control group, FBW-7 abundance increased obviously from 8 h to 24 h, and then FBW-7 abundance decreased three quarters from 24 hrs to 32 hrs. Under the disturbance of 50 nm nanoparticles, FBW-7 abundance was obviously lower than the control group in 8 hrs, and then FBW-7 abundance increased 4-folds from 8 hrs to 24 hrs and then decreased one half from 24 hrs to 32 hrs. Differently, being affected by 200 nm nanoparticles, FBW-7 abundance was significantly lower than the control group in 8 hrs. And then FBW-7 abundance increased quickly from 8 hrs to 24 hrs, and then dropped steeply from 24 hrs to 32 hrs.

Cell cycle changes and cell cycle regulator expression changes implicated how cells responded to and tried to overcome the effects of 50 nm and 200 nm nanoparticles. Among the three measured proteins, cyclin E was selected as a significant label of G1/S transition. 8 h was considered to be a time point of the middle G1 phase when cyclin E began to be synthesized, 24 hrs could be recognized as a time point of the late G1 phase or early S phase. In 32 hrs, cyclin E was mostly degraded in the middle-late S phase stage [19].

Thus, after co-incubated with 50 nm nanoparticles, p21 was consumed, and the synthesis and degradation of cyclin E were both retarded for hours. These results explained the G1 phase arrest in 24 hrs and S phase arrest in 48 hrs after cells were treated with 50 nm nanoparticles, and further proved that 50 nm nanoparticles could retard cell cycle progress. Therefore, 50 nm nanoparticles did cause mitochondria deformation (yellow dashed line in **Figure 3**), ROS release **(Figure 4a)**, but they triggered a p21-mediated self-repair process to prolonged G1 and S phase for cells to repair the damaged proteins and genome. So, the cell necrosis and G1 phase arrest relived in 48 hrs. Differently, after co-incubated with 200 nm nanoparticles, the hardly changed p21 abundance p21 had no contribution in the cellular responses to 200 nm nanoparticles. However, FBW-7 was downregulated to maintain cyclin E abundance and force cells to pass the G1/S transition, so that the un-repaired organelle and biomolecule damages were no longer repairable, and finally resulted in the increasing cell necrosis from 24 hrs to 48 hrs**(Figure 4b)**. Therefore, it could be deduced that when mitochondria internalized nanoparticles actively, cells could initiate an effective self-repair process, and the organelle and biomolecule damages were partially repairable. Whereas, when nanoparticles caused defects on the mitochondria membrane violently, cells could not initiate an effective self-repair process, and the organelle and biomolecule damages were non-repairable [20,21].

In the further step we culture zebrafish with different types of nanoparticles to study the teratogenesis from different cell damage and repair processes. It will be essential for understanding early zebrafish development especially in the process of neuro-development.

Animal experiments

The effects of 50 nm and 200 nm nanoparticles on the embryonic development of zebrafishes were presented in **Figures 7 and S5. Figure 7a** demonstrated the mutation frequencies of zebrafish eggs treated with 10 μg/mL 50 nm and 200 nm sulfhydride silica nanoparticles. According to the results, both 50 nm and 200 nm nanoparticles caused zebrafish egg mutations. The probable process of hatching enzyme inhibition were related to the nanoparticles internalizing through the chorion pore canals or the blocking of chorion pores due to the nanoparticles accumulation on the chorion surface and leading to oxygen supply shortage. From the SEM of Zebrafish eggs we found that both of the nanoparticles can attached on the surface of the eggs and entered into them result into different damage. While, 200 nm nanoparticles caused much more and severer mutations than 50 nm ones did. The results supported that 50 nm nanoparticles caused repairable cell injuries, especially genome and protein damages, in zebrafishes.

However, the cell injuries, as well as genome and protein damages caused by 200 nm nanoparticles, were unrepairable. **Figure 7b** presented the different innate abnormity of newly hatched zebrafishes under the effects of 50 nm and 200 nm nanoparticles. It was presented that after treated with 50 nm nanoparticle, multiple tumidities of abdomens can be found in zebrafishes (red rectangular in **Figure 7b**). However, after 200 nm nanoparticle treatment, zebrafishes had both tumidities in their abdomens (blue rectangular in **Figure 7b**) and nerve malformation at their back heads (dashed blue rectangular in **Figure 7b**). The results suggested that both 50 nm and 200 nm nanoparticles had toxicity during the embryonic development process, but 200 nm nanoparticles presented their toxicities on both neural system and viscus development, while 50 nm nanoparticles, presented their toxicities on viscus development.

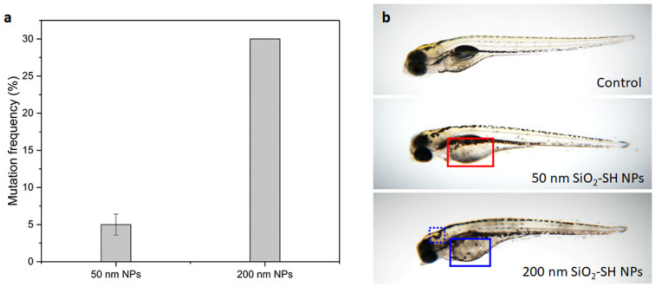

Figure 7: (a) Egg mutations of zebrafishes and (b) body malformations on hatched zebrafishes caused by 50 nm and 200 nm nanoparticles.

Discussion

In conclusion, different interaction processes between the nanoparticles and lipid membranes will result into different endocytosis kinetics. As show in the cartoon **(Figure 8)**, we mimic the intercellular pass way for different sized nanoparticles, 200 nm nanoparticles would scrape the mitochondria membrane violently, and at the same time the 50 nm nanoparticles could not flip or peel the monolayer of phospholipid membrane. The results of subcellular localization of the particles show that even though 200 nm nanoparticles scrape the mitochondria membrane, they cannot penetrate into the cells mitochondrion, but for 50 nm nanoparticles, they can be found in the cells mitochondrion without damage of the membrane. From the results, we deduced that 50 nm nanoparticles entered into the mitochondrion from protein dependent pass way. From the results of cell apoptosis and western blot we found that when the particles scrape the mitochondria membrane (200 nm), much serious ROS and large quantities of necrosis cells can be found. The non-repairable organelle and metabolism disorder resulted from decreasing of P21 should related with monolayer flip-flop of mitochondria membrane **(Figures 6 and 8a).** The cells interacted with endocytosis process of the 50 nm nanoparticles show better state **(Figures 4 and 5).** Self-repair process of cells can be found, it was suggested from abundant accumulation of P21 **(Figures 6 and 8b).** At the same time cell cycle can be found tend to similar with the control group after 24 hrs. Cells metabolism disorder process was reparable when intracellular nanoparticles entered into cells by protein depended pass way.

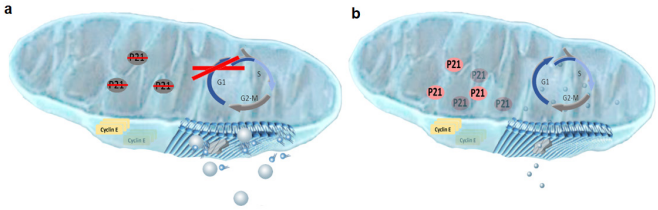

Figure 8: (a) 200nm particles pilled off the outer-leaflet of the cell and lead to P21 protein decrease; (b) 50nm nanoparticles penetrate the cells membrane from the protein depended pathway and lead to P21 protein accumulation.

Experiments of zebrafish helped us further understanding the toxicity effect of different particles, Organelle and biomolecule damages caused by 200 nm nanoparticles were non-repairable, that may relate to the damage of mitochondria membrane disturb. We found that the toxicity of 200 nm nanoparticles could not be eliminated and presented firstly on the neural system, the early developed system, and then on viscus, the later developed systems. We deduce from the results that the toxicities of 200 nm nanoparticles were maintained in the whole embryonic development, since the mitochondria membrane damage. However, the organelle and biomolecule damages caused by 50 nm nanoparticles were partially repairable; the toxicity of 50 nm nanoparticles was weakened in the stage of embryonic development. We suggested from the results that 50 nm nanoparticles enter mitochondria from the protein-assisted pass way that did not cause malignant neurodevelopmental abnormity but caused obvious viscus malformation as show in **Figure 7.** Optical strategy in this work helped us deeply understand the toxicity mechanism of different sized nanoparticles and to support safety assessment of nanoscale materials.

Conclusion

Mitochondria was highly related to the origin and development of various metabolic disorders, and mitochondria targeting nano-system designing as drug and drug deliverer, and it is an emerging strategy for various complex diseases. Therefore, deep digging of the interactions between nanoparticles and mitochondria would be illuminating for nano-scale drug design targeting to mitochondria. When the nanoparticles interact with cells, cell metabolic arrest and repair process were related with the particles size, surface charge but the possible mechanisms have not been widely investigated. This work we studied the interactions between mitochondria membrane and different sized nanoparticles. We found that when interacted with 200 nm particles, one leaflet of the cells membrane were teared off and this process led to cell metabolic block. Defects on the mitochondria membrane could not initiate a p21-mediated self-

repair process, nor be repaired by another mechanism, Irreversible cell damage and animal injury can be observed. Differently, 50 nm nanoparticles did not disturb the mitochondrial membrane structure but entered mitochondria in a mitochondrial-protein-dependent manner. Slight organelle and biomolecule damages can be found from *in vivo* experiments, but from the *in vitro* experiments, it can be observed that the damages could be partially repaired by p21 mediated self-repair process. The results suggest that the destruction of membrane structure by the particles will cause irreversible biological damage, and particles entering cells through protein assisted process will increase the expression of cell cycle related proteins and cells self-repair can be observed from the *in vitro* experiments.

This work demonstrated that the interaction models of mitochondria and nanoparticles could determine further cellular responses to nanoparticles, so the efficiencies of nano-scaled drugs could be enhanced by altering the interaction models of nano-systems and mitochondria. In the future, mitochondria membrane proteins would also be carefully explored to confirm their roles in the active mitochondrial uptake of nanoparticles and provide new channels for safe and effective mitochondria targeting drug delivery.

Appendix

Not applicable.

Acknowledgements

Thanks for the Southeast University and Nanjing Medical University Cooperation Project.

Funding

National Natural Science Foundation of China [No.11204033];

Availability of Data and Materials

All data and materials are included in the manuscript.

Ethics Approval and Consent to Participate

The authors declare that they approval and consent to participate.

Competing Interests

The authors declare that they have no competing interests.

Consent for Publication

Not applicable.

Authors' Contributions

Ting Wang, Guanwen Qu, and Chenglong Cai designed and performed the experiments, analyzed the data, and interpreted the results of experiments. Yaozhong Cheng, Zhewei Shuai, Boru You and Yixin Zhang performed the experiments, Zhangqi Feng, Jing Shang conceived and supervised the study. The manuscript was written by Ting Wang, Guanwen Qu and Chenglong Cai and revised critically by Ting Wang. All authors read and approved the final manuscript.

Authors' Information

Ting Wang and Guanwen Qu contributed equally to this work.

References

1. Kasumov EA, Kasumov RE,Kasumova IV (2020) Mild depolarization of the inner mitochondrial membrane is a crucial component of an anti-aging program. J Nov Physiother Phys Rehabil 7: 033-035.
2. Kim S, Nam HY, Lee J, Seo J (2020) Mitochondrion-targeting peptides and peptidomimetics: Recent progress and design principles. Biochem 59: 270-284.
3. Wang T, Deng Y, Chen Y, Qu G, Feng Z, et al. (2019) Disordered metabolism and repair mechanism: Mitochondria influenced by cationic and neutral nanoparticles. J Biomed Nanotechnol 15: 2428-2438.
4. Wang T, Qu G, Deng Y, Shang J, Feng Z, et al. (2019) Post-self-repair mechanism of neurons cells under the influence of neutral and cationic nanoparticles. Chin Chem Lett 30: 2368-2374.
5. Wang T, Deng Y, Qu G, Cheng Y, Shang J, et al. (2019) Micro-array chip system for accurate, rapid diagnosis and target treatment of breast cancer cells SK-BR-3. Chin Chem Lett 30: 1043-1050.
6. Rossi S, Donati, Fontana L, Porcaro F, Battocchio C, et al. (2016) Negatively charged gold nanoparticles as a dexamethasone carrier: Stability in biological media and bioactivity assessment in vitro. RSC Adv 6: 99016-99022.
7. Lee SY, Cho HJ (2019) Mitochondria targeting and destabilizing hyaluronic acid derivative-based nanoparticles for the delivery of lapatinib to triple-negative breast cancer. Biomacromolecules 20: 835-845.
8. Wang T, Li DW, Lu XL (2011) Single lipid bilayers constructed on polymer cushion studied by sum frequency generation vibrational spectroscopy. J Phys Chem 115: 7613-7620.
9. Wang T, Feng ZQ, Wang C, (2018) Real-time investigation of interactions between nanoparticles and cell membrane model. Colloids Surf B Biointerfaces 164: 70-77.
10. Ding B, Jasensky J, Li Y, Chen Z (2016) Engineering and characterization of peptides and proteins at Surfaces and Interfaces: A case study in surface-sensitive vibrational spectroscopy. Acc Chem Res 49: 1149-1157.
11. Ye SJ, Li HC, Yang WL, Luo Y (2014) Accurate determination of interfacial protein secondary structure by combining interfacialsensitive amide I and amide III spectral signals. J Am Chem Soc 136: 1206-1209.
12. Guo L, Wang T, Chen Z, He N, Chen Y, et al. (2018) Light scattering based analyses of the effects of bovine serum proteins on interactions of magnetite spherical particles with cells. Chin Chem Lett 29: 1291-1295.
13. Fattal E, Parente RA, Nir S, Szoka FC (1992) Phospholipid flip-flop induced by membrane-associated peptides. Congr Int Technol Pharm 5: 70-81.
14. McIntyre JC, Sleight RG (1991) Fluorescence assay for phospholipid membrane asymmetry. Biochem 30: 11819-11827.

15. McNamee MG, McConnell HM (1973) Transmembrane potentials and phospholipids flip-flop in excitable membrane vesicles. Biochem 12: 2951-2958.

16. Anzai K, Yoshioka Y, Kirino Y (1993) Novel radioactive phospholipid probes as a tool for measurement of phospholipid translocation across biomembranes. Biochim Biophys Acta 1151: 69-75.

17. Liu J, Brown KL, Conboy JC (2013) The influence of cholesterol on the intrinsic rate of lipid flip–flop as measured by sum-frequency vibrational spectroscopy. Faraday Discuss 161: 45-61.

18. Cuypers W, Hermens T (1986) The role of intrinsic binding rate and transport rate in the adsorption of prothrombin, albumin and fibrinogen to phospholipid bilayers. J Colloid Interface Sci 111: 544-554.

19. Higuchi Y (2013) Chromosomal DNA fragmentation in apoptosis and necrosis induced by oxidative stress. Biochem Pharmacol 66: 1527-1535.

20. Festjens N, Berghe TV, Vandenabeele P (2016) Necrosis-a well-orchestrated form of cell demise: Signaling cascades, important mediators and concomitant immune response. Biochim Biophys Acta Bioenerg 1757: 1371-1387.

21. Spruck CH, Won KA, Reed SI (1999) Deregulated cyclin E induces chromosome instability, Kinase-independent function of cyclin E. Nature 401: 297-300.